

THE PENNSYLVANIA STATE UNIVERSITY
SCHREYER HONORS COLLEGE

DEPARTMENT OF NUCLEAR ENGINEERING

In-Situ Analysis of Dispersion Strengthened Tungsten Alloys and the Effect of Dispersoid
Population on the Areal Density of Helium Bubble Nucleation

EVAN LAMBERT
SPRING 2022

A thesis
submitted in partial fulfillment
of the requirements
for a baccalaureate degree
in Nuclear Engineering
with honors in Nuclear Engineering

Reviewed and approved* by the following:

Dr. Jean Paul Allain
Department Head of Nuclear Engineering
Thesis Supervisor

Dr. Elia Merzari
Professor of Nuclear Engineering
Honors Adviser

* Electronic approvals are on file.

ABSTRACT

Nuclear fusion has long been a proposed form of energy creation; however, it always has its shortcomings whether that be in confinement technology, magnetic technology, etc. In 2025, the ITER tokamak will begin operation as the world's largest experiment in nuclear fusion. This massive machine undergoes extraordinarily harsh conditions of high heat flux and high particle flux. A region within the reactor that experiences a particularly high particle flux is called the divertor. The divertor of ITER will be made mostly of stainless steel with a thin tungsten coating to assist in protection of high energy ions. The properties of pure tungsten are desirable for implementation into the harsh environment inside of a tokamak; however, helium atoms at high fluxes are known to nucleate within the tungsten as bubbles which in turn, burst, damaging the material and creating less desirable physical properties. Advanced tungsten alloys such as dispersion strengthened tungsten have been proposed as a means to combat or slow down the rate of helium bubble nucleation. In this work, a 5-weight percent tantalum carbide dispersion strengthened tungsten was analyzed with an in-situ TEM facility dosed with a fluence of 2 keV helium ions. 4 regions were selected and the areal helium bubble density was counted as a function of fluence. It was found that the presence of the carbide dispersoids overall lowers the density of helium bubbles while the presence of bubbles in the dispersoids themselves is nonexistent.

TABLE OF CONTENTS

LIST OF FIGURES	iii
LIST OF TABLES	iv
ACKNOWLEDGEMENTS	v
Chapter 1 Introductory Information.....	1
1.1 Nuclear Fusion	1
1.2 Tokamaks and ITER	6
1.3 First Wall, Divertors, and Some Serious Damage	9
1.4 Particle and Plasma Material Interactions.....	12
Chapter 2 Tungsten's Interactions with Plasma and Potential Solutions	14
2.1 Tungsten.....	14
2.2 Advanced Tungsten Alloys and Dispersion Strengthened Tungsten	19
Chapter 3 Experiment and Methods	22
3.1 Material and Experimental Methods	22
Chapter 4 Results and Discussion.....	24
Chapter 5 Summary and Conclusions.....	32
References.....	33

LIST OF FIGURES

Figure 1. A plot of nuclear binding energy per nucleon as a function of the number of nucleons. The binding energy per nucleon increases as a function of the number of nucleons and reaches a maximum at Fe-56, then slowly drops as elements get more massive [25].2	2
Figure 2. A plot of the fusion reactivity (average cross section times relative speed of reacting nuclei) vs. temperature for three nuclear fusion reactions [8].....4	4
Figure 3. The Proton-proton fusion process that occurs in the sun [1].5	5
Figure 4. Deuterium-tritium fusion process that will occur in grid connected fusion reactors [9]. 6	6
Figure 5. ITER uses both toroidal (on the left) and poloidal (on the right) magnets that help confine the plasma. The coils will reach a power of 11.8 Tesla and 6 Tesla respectively [13].7	7
Figure 6. The major plasma regions in a cross section of a tokamak plasma. Due to the open magnetic flux lines from beyond the separatrix, large depositions of particles fall into the divertor strike points [17]. 10	10
Figure 7. A CAD representation of an ITER divertor cassette. Each part of the PFC of the divertor is highlighted with its use as discussed [16]. 11	11
Figure 8. The principal mechanisms of PMI and their physical impact on PFC surfaces [22]. 13	13
Figure 9. Examples of different types of point defects [23]. 16	16
Figure 10. Helium bubbles within a sample of 5 wt. % W-TaC sample used in the experiment. 17	17
Figure 11. A top down and side profile view of tungsten fuzz formation post helium irradiation [26]. 18	18
Figure 12. Schematic of a typical SPS device used in surface alloy manufacturing [34].20	20
Figure 13. DS-W lamella used for the <i>in-situ</i> helium ion irradiation experiment.23	23
Figure 14. The four different locations investigated for areal helium bubble density. Area 1 has one visible grain boundary and W bulk, Area 2 consists of high density W-W grain boundaries, Area 3 is mostly W bulk with no visible grains, and Area 4 consists of pores in the lamella along with W-W grain boundaries.....23	23
Figure 15. Figure of Areal Helium Bubble Density vs. Ion Fluence.25	25
Figure 16. Area 1 Evolution for each fluence step starting at 0 ions/cm ²26	26
Figure 17. Area 2 Evolution for each fluence step starting at 0 ions/cm ² (Images enhanced with +20% brightness and -40% contrast).26	26
Figure 18. Area 3 Evolution for each fluence step starting at 0 ions/cm ²27	27

Figure 19. Area 4 Evolution for each fluence step starting at 0 ions/cm ²	27
Figure 20. Each Area at the maximum fluence of 1E16 ions/cm ² . Area 4 has noticeably smaller bubbles than the other 3 Areas (Area 2 was changed to have +20% brightness and -40% contrast).....	28
Figure 21. Helium bubble growth and migration is more common at the W-W grain boundaries as seen in this snip from Area 1.....	29
Figure 22. TaC dispersoid within the DS-W-TaC alloys used in the experiment. There are no obvious helium bubbles within it, but they can be seen in the surrounding tungsten.	30
Figure 23. W nanofiber growth on the specimen.....	31

LIST OF TABLES

Table 1. Areal Bubble Densities for Each Chosen Area.....	25
---	----

ACKNOWLEDGEMENTS

I would like to acknowledge Dr. J. P. Allain. Without meeting and working Dr. Allain, I would not have found my love and passion for this field. Moreover, I would like to thank the many faculty at the Ken and Mary Alice Lindquist Department of Nuclear Engineering. Their patience and teaching excellence provide a fantastic environment for learning and growth into amazing engineers and researchers. Finally, I would like to thank my friends and family. Without the love and support of them, many of my achievements would not have been possible.

Chapter 1

Introductory Information

This chapter outlines the physics and the goals of nuclear fusion. The fusion process, tokamak reactors, the ITER tokamak, plasma facing components (PFCs), an introduction to plasma material interactions and the problems encountered with plasma-surface interactions (PSI).

1.1 Nuclear Fusion

The sun and all other stars within our universe exert an enormous gravitational force onto the material within them. The heat and force on the atoms within a star are so much, the material becomes an ionized gas called a plasma and undergoes nuclear fusion [1]. Nuclear fusion is the combining of two nuclei into a new nucleus of a different, heavier atom. However, during this process, it is seen that the new fused atom's total mass is actually less than the combined mass of the two atoms that constituted it through the nuclear reaction. The difference of mass between the products and reactants is called the mass defect. This seemingly missing mass is transformed into energy based on Einstein's Energy-Mass Equivalence equation seen below in Eq 1.1. This energy from mass transformation is the source of energy that will be utilized in future fusion reactors for electrical power and is what is currently used in fission reactors.

$$E = mc^2 \tag{1.1}$$

Fusion is more energetically favorable for atoms of lower nuclei per nucleus. This is due to something called nuclear binding energy. Nuclear binding energy is the energy that keeps the nucleus of an atom from breaking into its component parts. The trend of binding energy per nucleon is seen in Figure 1. As the number of nuclei within a nucleus is increased, the nuclear binding energy increases drastically up to Fe-56 which has the highest binding energy per nucleon. The two ends of this curve can be exploited for energy. As of 2017, 11% of the world's electricity come from a type of exploitation of binding energy called nuclear fission [2]. Fission occurs when the nucleus of an atom is too unstable and the nucleus breaks apart into two smaller pieces called fission products. The elements used in fission have a high nuclei per nucleus count and are seen on the right side of the curve where the nuclear binding energy per nucleon begins to decrease. This process releases energy as there is again a mass difference between the original atom and the

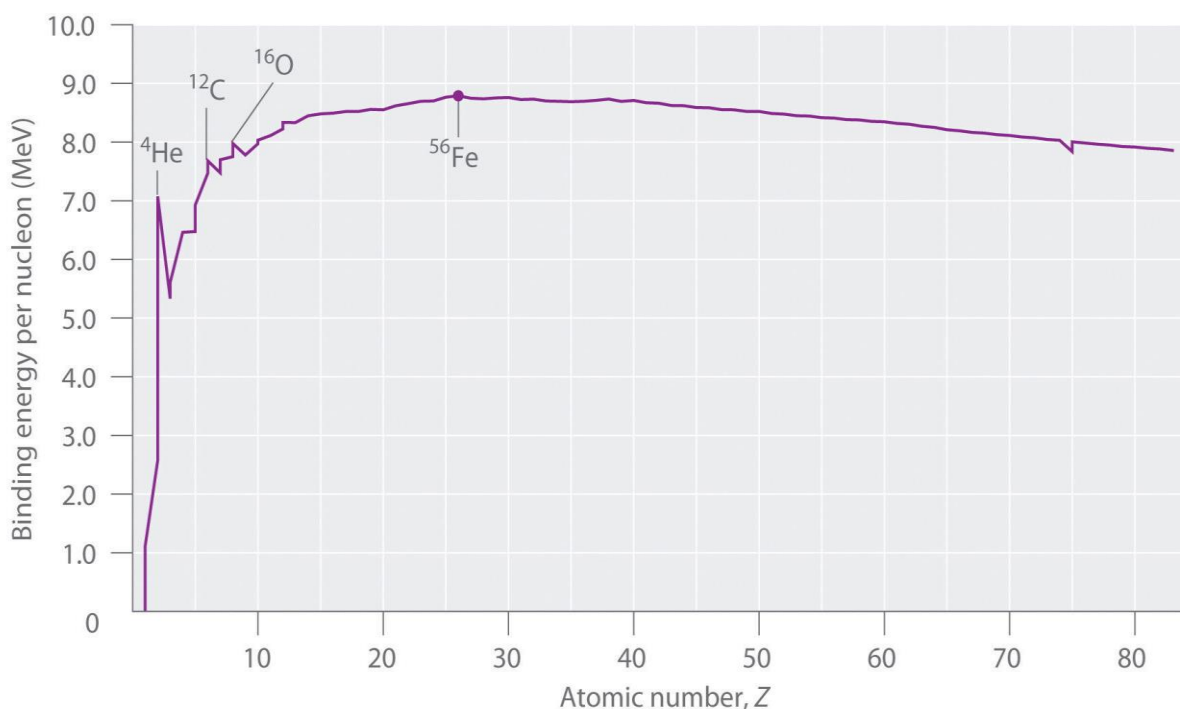


Figure 1. A plot of nuclear binding energy per nucleon as a function of the number of nucleons. The binding energy per nucleon increases as a function of the number of nucleons and reaches a maximum at Fe-56, then slowly drops as elements get more massive [25].

two products that are born from the split which is utilized for electrical power generation [3]. As mentioned earlier, the other way to exploit the energy stored within a nucleus is through the fusing of two atoms.

For fusion to occur, it is optimal to use light nuclei which are pictured on the left side of Figure 1. Nuclear fusion is a sort of tug-o-war between two forces: the electrostatic force and strong force. Inside of a nucleus are protons and neutrons where neutrons are neutral in charge, but protons are positive in charge. The more protons that are within a nucleus, the greater the Coulombic repulsion force will be when trying to fuse atoms which is why lighter elements like hydrogen are more optimal to use as they have a low number of protons (just one in hydrogen's case). The other force at play is the strong force. At extremely short inter-nucleic distances, nucleons strongly attract each other. It is more favorable to have more nucleons to increase this force of attraction. So, if the electrostatic force between protons is overcome, then the strong force will attract the nuclear particles together in a fusion reaction which is why the deuterium-tritium (D-T) reaction has taken the stage as the fusion reaction to be implemented in commercial reactors [4].

Nuclear fusion is a quantum mechanical process and is therefore probabilistic in nature. The probability for a fusion reaction to take place is called a cross section. This cross section depends on both the temperature and density of a fusion plasma. For D-T fusion, the cross-section peaks over 100 million Kelvin as seen in Figure 2. Because fusion devices on Earth are low density, it is best to approach this extremely high temperature to have the highest probability a fusion reaction will occur [5]. This is in contrast with the sun which is at a much lower temperature of 15 million Kelvin but a much higher density [6]. The high density of the sun from extreme gravitational forces combined with the temperature is enough to increase the cross section of

hydrogen-hydrogen fusion reaction as seen in Figure 3. As mentioned earlier, the conditions inside fusion reactors and the sun create an ionized gas also known as a plasma. This differs from a gas as the motion of fusion plasmas is dictated more so by electromagnetic forces than by inertial collision forces [7].

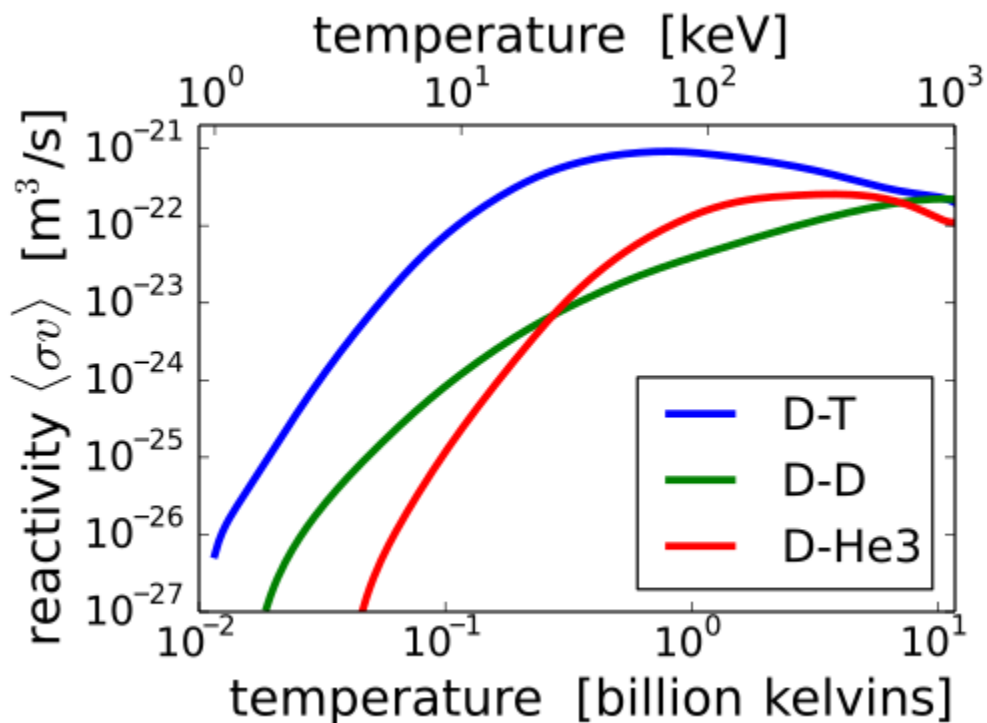


Figure 2. A plot of the fusion reactivity (average cross section times relative speed of reacting nuclei) vs. temperature for three nuclear fusion reactions [8].

Planned nuclear fusion reactors will use deuterium-tritium (D-T) fusion where deuterium is an isotope of hydrogen with one proton and one neutron and tritium is an isotope of hydrogen with one proton and two neutrons. Other reactions such as deuterium-deuterium (D-D) are planned to be used in experimental reactors.

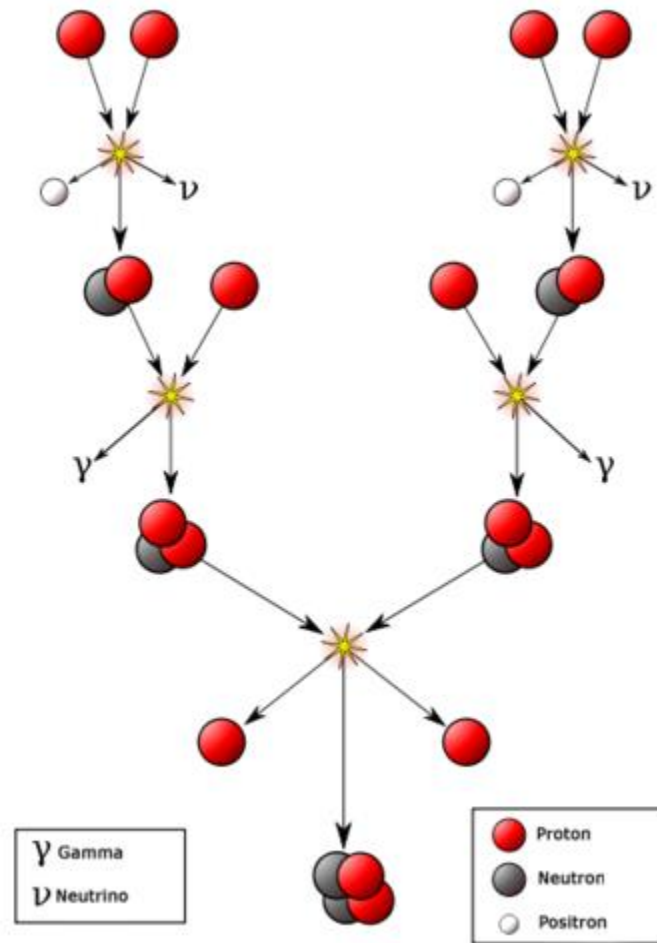


Figure 3. The Proton-proton fusion process that occurs in the sun [1].

The D-T fusion reaction produces helium-4 (an alpha particle) and a neutron as seen in Figure 4.

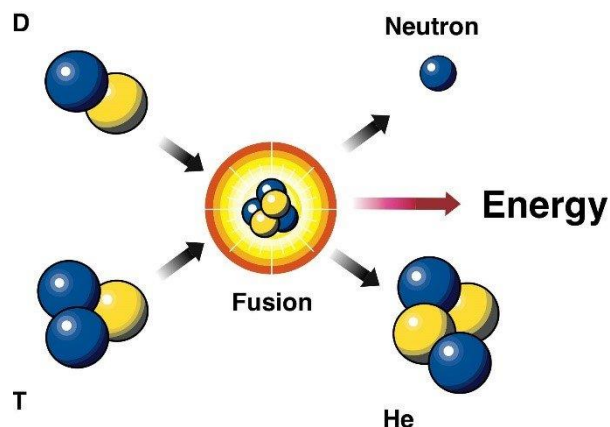


Figure 4. Deuterium-tritium fusion process that will occur in grid connected fusion reactors [9].

This reaction produces about 17.6 MeV of energy. Whereas D-D fusion releases about 4 MeV per fusion and U-235 fission produces 200 MeV per reaction. When normalized by mass, the D-T fusion reaction produces over four times as much energy as the uranium fission reaction [10]. This massive release of energy is carried away by the alpha particle and the neutron. The neutron itself carried about 14 MeV of energy away from the reaction and induces major structural damage to the physical walls of fusion reactors which will be discussed later. The energy released from this will be captured as heat and then made into electrical energy.

1.2 Tokamaks and ITER

Currently, the field of nuclear fusion is dominated by research in two main areas: Inertial Confinement Fusion (ICF) and Magnetic Confinement Fusion (MCF) reactors. ICF utilizes high energy lasers focusing their energy onto a tiny capsule, called a hohlraum, to create very hot and very dense plasmas to induce nuclear fusion over small time scales in order to understand the very high density fusion plasma environment [11]. MCF on the other hand uses strong magnetic fields to confine a diffuse plasma over larger time scales to induce the D-T fusion reaction.

The most advanced type of MCF reactor is known as a tokamak. The concept of the tokamak stretches back all the way to the 1950s Soviet Union nuclear program [12]. The tokamak is known as a toroidal type MCF reactor. It utilizes a toroidal magnetic field geometry to reduce boundary losses of the plasma as seen in Figure 5. Using a curved field geometry does create its own challenges. The curvature of the field creates a non-zero gradient causing a drift of ions and electrons from their toroidal orbits. This drifting creates an electric field which in turn creates a Lorentz Force stemming from Eq. (1.2)

$$\mathbf{F} = q\mathbf{E} + q\mathbf{v} \times \mathbf{B} \quad (1.2)$$

To counteract this drifting, a poloidal field is also applied. This results in the ions and electrons traveling in helical orbits around the reactor.

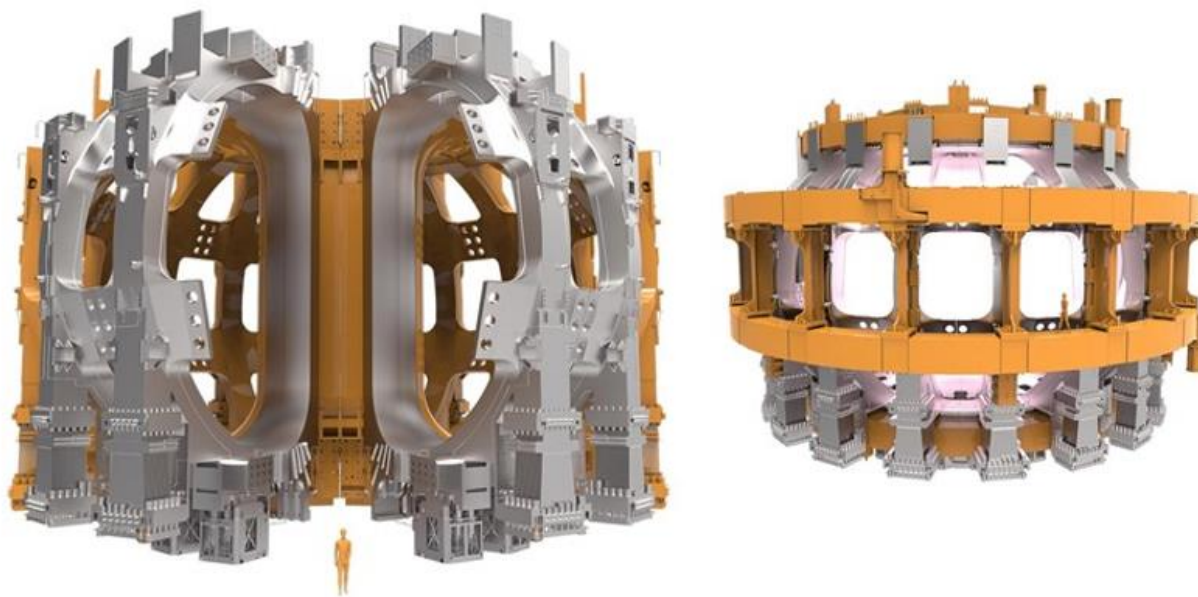


Figure 5. ITER uses both toroidal (on the left) and poloidal (on the right) magnets that help confine the plasma. The coils will reach a power of 11.8 Tesla and 6 Tesla respectively [13].

To get to such high temperatures necessary for fusion, a combination of ohmic heating from the toroidal plasma current (essentially how a toaster heats food), neutral beam injection, and radio frequency waves are used. A goal of planned experimental tokamaks like ITER is to create a burning plasma. This type of plasma is self-sustaining and can effectively keep itself at temperatures necessary for fusion to occur [5].

There have been many tokamak experiments throughout the late 20th century and early 21st century. Fusion science has continuously improved since its inception with many reactors achieving new research goals they were set out to do so. This all culminates in the world's largest science experiment since the Large Hadron Collider: ITER. It is a joint project between the US, EU, Japan, Russia, India, China, and South Korea to demonstrate and test fusion technologies that will be needed to operate a fusion power plant. Construction for ITER has been underway since 2010 and is expected to have a power amplification value of more than 10 with first plasma occurring in 2025 assuming no further delays [14].

To reiterate, ITER is an experiment with the purpose of testing decades worth of tokamak improvements and technologies with the main goal of showing fusion is capable of exceeding net power. There are currently four major critical engineering issues with a fusion pilot plant that ITER will help address: tritium production and a closed tritium fuel cycle, thermal power exhaust and energy generation, remote handling and operation of the reactor, and material irradiation damage which will be discussed more thoroughly in this report.

1.3 First Wall, Divertors, and Some Serious Damage

Inside of the toroidal chamber of ITER, temperatures will exceed 150 million degrees Celsius through the aforementioned ohmic heating, neutral beam injection, and radio frequency waves [15]. Along with high temperature (though not nearly as high as the plasma's center), the first wall layer of ITER will experience plasma-to-surface contact. The plasma material interactions (PMI) and high particle flux on the walls will lead to severe erosion, and the contamination of the burning plasma. One main design feature to avoid a large erosion toll on the wall layers of tokamaks is the divertor. A divertor is a surface that extends into the plasma to intersect the magnetic field lines and allow for plasma flow into this region as the plasma diffuses out of the core. As one can imagine, the divertor of a tokamak experiences a very large fluence of particles over its life time. ITER's divertor will consist of 54 cassette assemblies situated at the bottom of the toroidal reactor as seen in Figure 6.

The divertor cassettes feature a baffled Inner Vertical Target (IVT) and Outer Vertical Target (OVT), inner and outer reflector plates, and a dome structure situated below the x-point which separates the inner and outer parts of the divertor as seen in Figure 7. The divertor cassettes of ITER are made of steel support structure protected by a layer of tungsten (W) armor. Throughout the life of the divertor, each cassette will experience extraordinary temperatures and particle fluence. Heat flux expected onto the surface of the IVT and OVT are around 10 MW/m^2 with higher peak values being experienced during certain plasma events such as an Edge Localized Mode (ELM). An ELM occurs as a sort of explosive instability during which the plasma violently discharges particles returning it to a more stable state [16]. Originally, the divertor cassette shield was to be made of both a carbon fiber composite (CFC) and W, but due to the extreme conditions, it was decided that a full W shield was necessary as the CFC introduced too many impurities into

the plasma resulting in more wall damage through PMI and plasma disruptions [16]. The damage types involved will be introduced and discussed in the next section

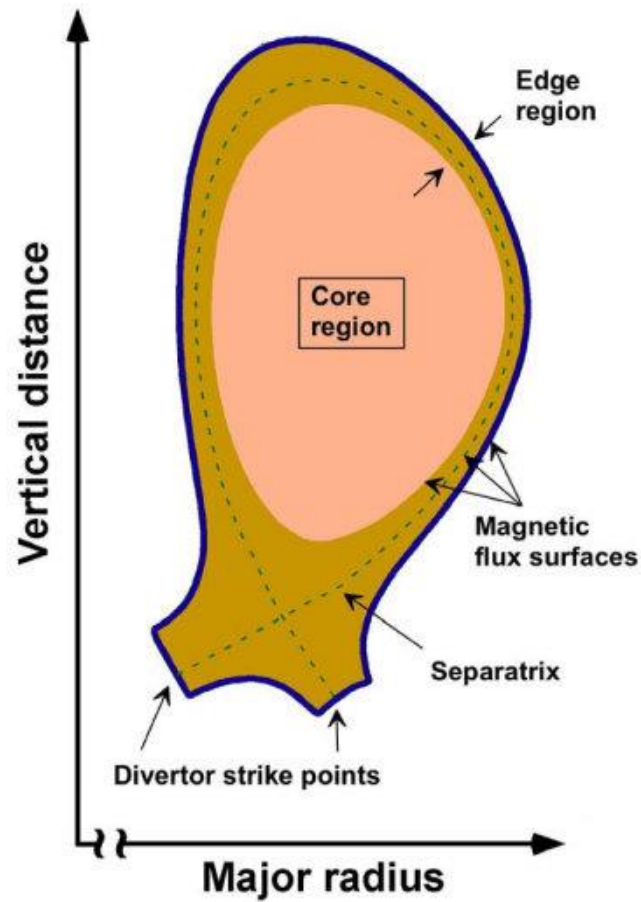


Figure 6. The major plasma regions in a cross section of a tokamak plasma. Due to the open magnetic flux lines from beyond the separatrix, large depositions of particles fall into the divertor strike points [17].

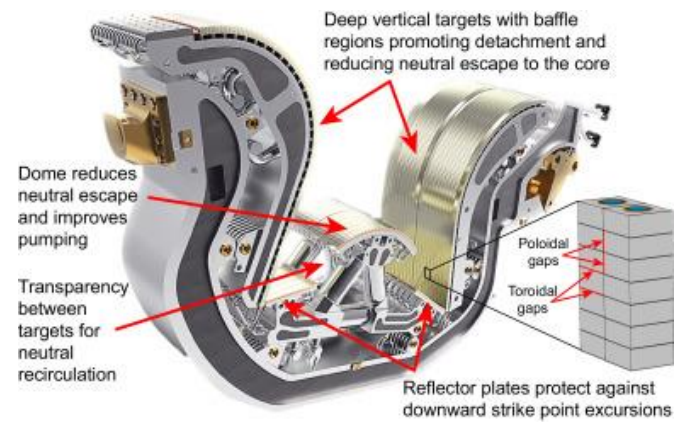


Figure 7. A CAD representation of an ITER divertor cassette. Each part of the PFC of the divertor is highlighted with its use as discussed [16].

1.4 Particle and Plasma Material Interactions

As discussed earlier, one of the biggest engineering challenges of demonstrating tokamaks as a viable source of electrical power is overcoming damage induced by PMI. A simplified view of PMI involves particles escaping the core plasma by passing over the separatrix and striking the containment wall. These particles are a mix of energetic ions which collide with atoms along the surface and implant themselves not very deeply. Only up to tens of nanometers [18]. These energetic ions can in turn release atoms from the wall material that was struck in an event called sputtering. These sputtered atoms can become impurities in the core plasma taking energy away from the ions needed for fusion to happen. The actual mechanisms involved in PMI are much more complicated and are outlined somewhat in Figure 8 and are further complicated by high energy neutrons which attenuate deep into the wall structure. Over time, the blasting of particles onto the walls of a tokamak damage the surface by inducing chemical erosion, undergoing physical sputtering, creating vacancies, becoming interstitial atoms, forming dislocation loops, etc.

Each PMI process operates at different temporal and spatial scales which even further complicates the matter. After being exposed to a fusion plasma, a surface can be expected to appear nothing like the material that was put inside as a PFC in the first place. The prime challenge of creating a vessel for a fusion reactor is to build an understanding of PMI and then develop materials that are capable of withstanding the harsh environment that they are placed in. Many aspects PMI are understood which led to the decision to build the divertor of ITER out of W. However, there are still consequences of PMI that need to be addressed with the materials chosen. As seen in Figure 3, helium is a product of the D-T fusion process as an alpha particle. These helium particles pose a huge engineering problem to the W divertor targets. Once embedding into the near surface matrix of the tungsten, they become highly mobile interstitial atoms. As the W heats up from

plasma heat flux exposure, the helium atoms migrate out from the surface inducing more surface damage which will be discussed further in the Chapter 2.

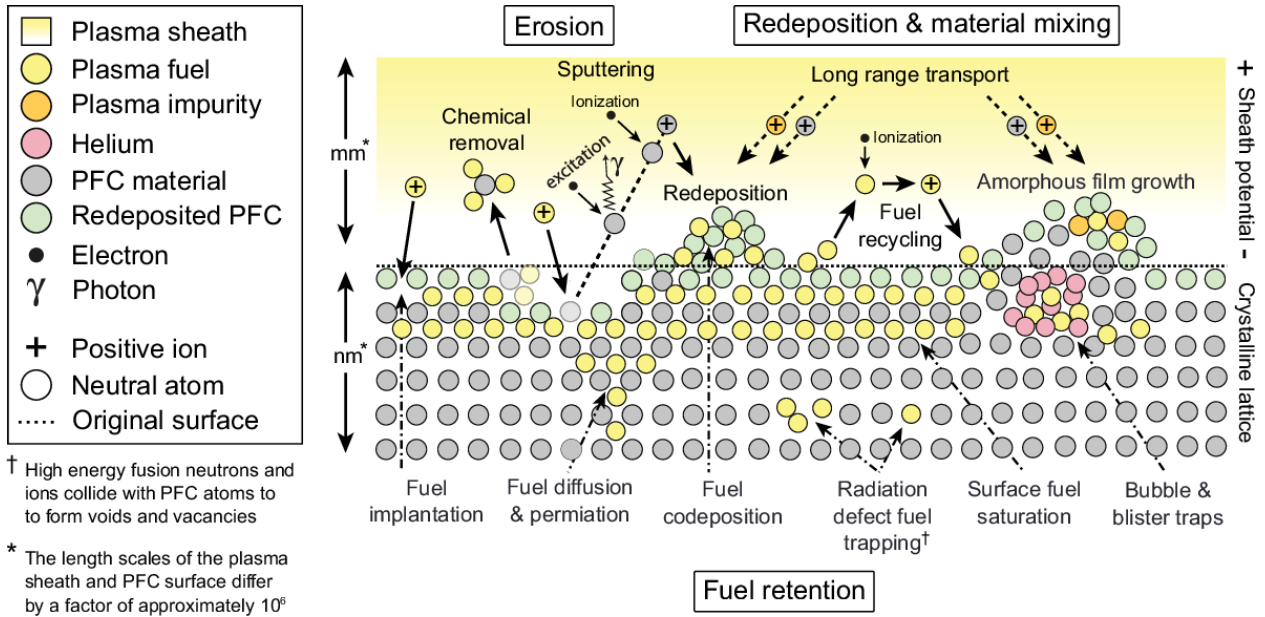


Figure 8. The principal mechanisms of PMI and their physical impact on PFC surfaces [22].

Chapter 2

Tungsten's Interactions with Plasma and Potential Solutions

W has become the main proposed armor for the ITER divertor after many years of research tokamak-based physics simulations codes based on ITER [16]. The desired properties of tungsten that make it a desirable material for MCF plasmas will be discussed as well as its setbacks, and a proposed new alloy to assist in the helium capture problem discussed above: Dispersion Strengthened Tungsten alloys (DS-W).

2.1 Tungsten

W has many characteristics which have sparked interest in materials scientists and MCF researches as a main candidate for protection of the divertor in ITER and many other upcoming tokamak experiments. Due to the extreme temperature and high heat flux environment, a high melting point temperature is easily a desired trait for PFC materials to possess and W has the highest melting point temperature of any pure material currently known [19]. W also possesses both a high thermal conductivity and a low coefficient of thermal expansion allowing it to not cause much mechanical stress in components while heated and allow for easy mechanisms of cooling as it does not trap heat. W is also relatively chemically stable and is high heat resistant [20].

Along with these thermomechanical and chemical properties, W has many desired PMI properties desired for a first wall material in fusion reactors. W has a high sputtering threshold and a low sputtering rate allowing for overall lower sputtered atoms from the W wall surface. With a lower number of sputtered atoms, less kinetic energy will be lost from the fusion D-T fusion

plasma to higher Z elements. This is an almost necessary requirement for W as it is a high Z element. High Z elements take more kinetic energy away from collisions in the plasma when compared to low Z elements. To continue, W also has a low deuterium/tritium retention which paves a way into fuel recycling for D-T ions that escape the core plasma. Furthermore, W has adequate corrosion resistance and lacks hydride formation [20].

Along with the advantages listed above, W is also resilient in regards to neutron irradiation. Under neutron irradiation, the thermal conductivity of W does not decrease as sharply as other materials. Moreover, W is not affected greatly by neutron activation of high energy neutrons expected from nuclear fusion meaning it is unlikely to absorb the fusion neutrons and undergo a transmutation reaction [21].

Although the behavior of W in a fusion environment is naturally advantageous based on the information discussed above, it has a number of important shortcomings that must be addressed before the commercialization of MCF reactors. Mechanically, W is a very brittle material with a high ductile-to-brittle temperature (DTBT). Being a brittle material complicates the fabrication and machining process of the W components in tokamaks. The brittle nature of W is only made worse by the neutron irradiation which increases the DTBT even further [20].

Along with the neutron irradiation problem, W also faces the hurdle of a massive PMI issue: high helium retention. Helium (He) is created as a byproduct of the D-T fusion reaction as discussed above. These He ions will implant themselves into the W divertor armor and begin to cause physical within its lattice. He is characterized by its fast thermal migration within metals meaning that the individual atoms will move quickly to find point defects to settle into. These point defects are vacancies in the metal lattice (a missing atom in the lattice) or interstitial atoms that are trapped within the metal lattice as seen in Figure 9. When W is irradiated with He in the keV

range, the number of implanted He atoms is comparable to the number of radiation induced point defects [22]. This means the He radiation induces damage onto a metal surface when implanting and then gets trapped in the induced damage areas. This damage that is caused by the He irradiation is located in the sub-surface region of the bulk which is up to 10 nm [22].

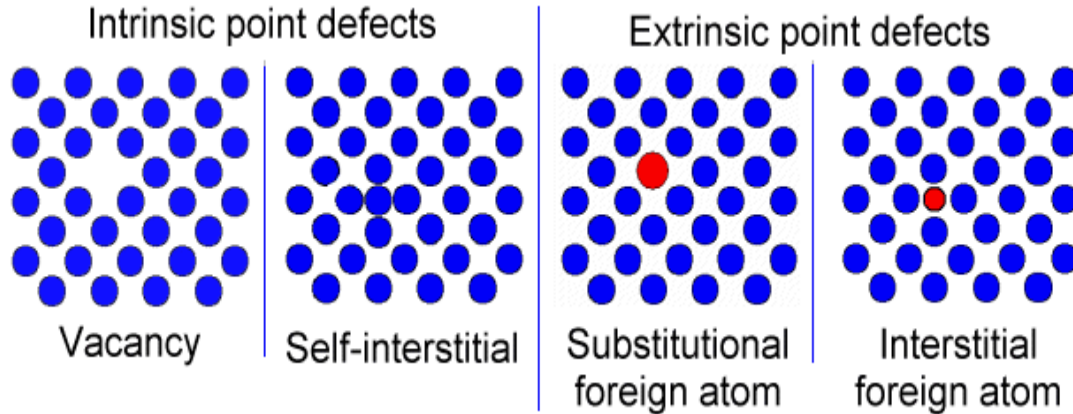


Figure 9. Examples of different types of point defects [23].

Regarding W specifically, the incident energy of the He ions must be higher than a threshold energy to displace a W atom from its lattice. Once this occurs, the previously described point defects can begin to form in a small range just beneath the surface up to 10 nm. Because W has a low migration energy (or energy for point defects to move within the bulk material), interstitial He atoms can thermally migrate even at room temperature and form interstitial dislocation loops [22]. These are large numbers of interstitials creating an extra plane within the lattice of the W surface. With further irradiation, these dislocation loops grow larger and accumulate the less mobile point defects as they also continue migration. From here, the He conglomeration will begin to form bubbles as seen in Figure 10. Although low energy He irradiation will not be able to cause damage and point defects through collisions, it will still implant into the W surface and form bubbles at interstitials and interstitial loops (a dislocation loop of

interstitials). The size of the bubbles is very temperature dependent and in general, larger bubbles form at higher temperatures as the migration energy barrier become lower [22].

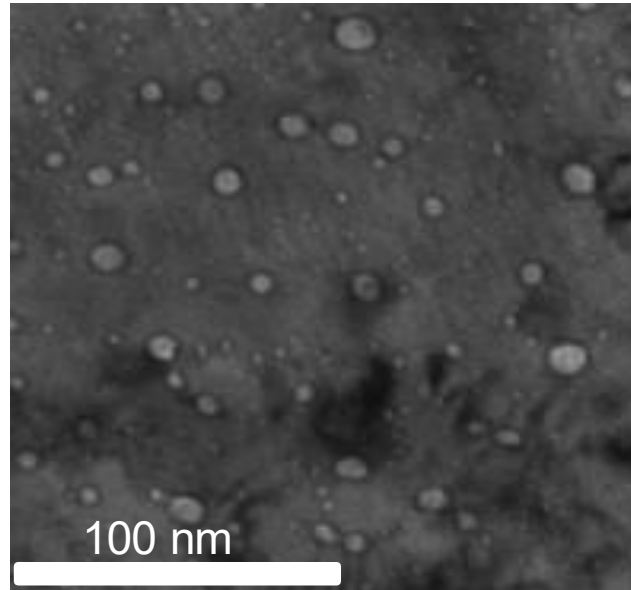


Figure 10. Helium bubbles within a sample of 5 wt. % W-TaC sample used in the experiment.

Once these bubbles form within the W bulk, they will eventually migrate to the surface and cause blistering or burst [24]. These events lead to temperature dependent surface modifications: pitted surfaces below 1000K, a *fuzz* nanostructure observed between 1000K and 2000K, and micrometer-sized holes above 2000K [24]. The fuzz formation can be seen in FIGURE HERE. This growth has been observed on the Alcator C-Mod tokamak's divertor paving the way for the needs to research the PMI and thermomechanical changes that are induced by these structures [25].

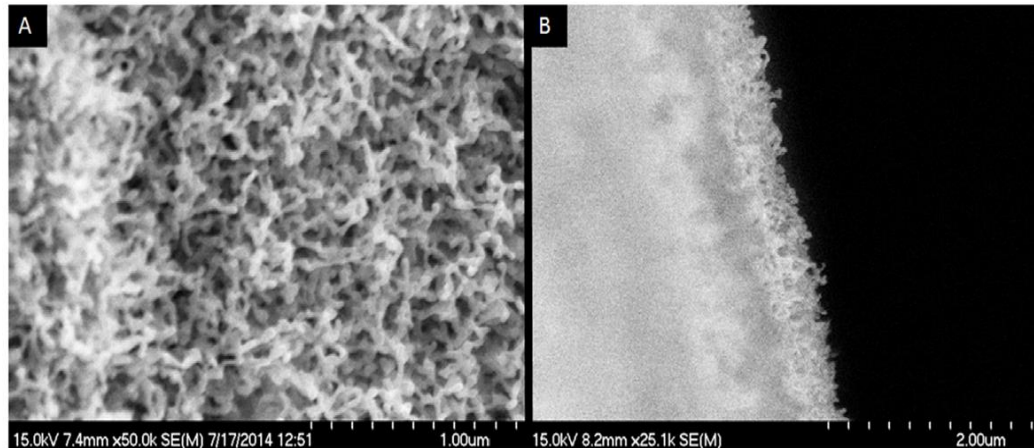


Figure 11. A top down and side profile view of tungsten fuzz formation post helium irradiation [26].

As one can imagine, the growth of the *fuzz* or fiberform nanostructures causes various changes to the physical properties of the W surface. With nanostructuring, the surface area of W can increase by up to a factor of 30 with a *fuzz* thickness of a few microns. This increase in surface area can lead to increased hydrogen deposition and therefore retention onto the W surface [27]. Along with this change, these nanostructures also decrease the sputtering rate [28], reduce particle reflectivity which increases the power transferred to the surface [29], and significantly decrease the thermal conductivity [30]. Although the growth of the *fuzz* has both positives and negatives for use as a PFC, it is preferred that the mechanical properties and PMI properties of what is initially put into a tokamak remains constant over its life cycle. To combat the formation of the nanofibers and the trapping of helium within W, solutions are proposed which will be discussed in the next section.

2.2 Advanced Tungsten Alloys and Dispersion Strengthened Tungsten

Increasing the lifetime of PFCs in a tokamak is important to reduce the number of repairs that will need to be done over the lifetime of each component. However, it is impractical to search for a material that will survive countless years inside of a fusion reactor without any repairs being made. So, a tradeoff of longevity of devices/materials and their ease of repair is something consistently researched in the field of fusion materials. Another important consideration is the fact that W will serve as a protection layer for the divertor and not the main material component of the PFC. This opens up avenues for W alloy processes that only create thin surfaces as the PMI properties are very surface level.

As W alloys and materials are designed, they are tested for both their He retention as well as how He migrates out of the bulk and out of the surface. For He retention's case, materials that have large numbers of defect sinks to attract the interstitial atoms along grain boundaries are looked at such as ultrafine and nanocrystalline W [31], high entropy alloys [32], and also the aforementioned DS-W alloys [33].

DS-W alloys are W that have an evenly dispersed number of second phase carbide grains throughout. The ones currently investigated for the purposes of use as a PFC have Titanium Carbide (TiC), Zirconium Carbide (ZrC), and Tantalum Carbide (TaC) of varying wt. percent up to 10%. These alloys are manufactured through a process called Sparc Plasma Sintering (SPS). SPS is a fast sintering technique characterized by the use of uniaxial pressure and high-intensity, low-voltage, pulsed current at the same time. During the process, ceramic carbide powders are distributed onto a W surface of which an electrical discharge between the powder particles is created which creates localized plasmas between particles heating said particles to several thousand degrees [34]. This heating causes impurity vaporization out of the surface and the

particles melt and fuse creating necks between each other. Next, a DC pulse is fed through the material which further connects the newly formed necks from the plasma heat. The heat from the DC pulsing increases the diffusion of particles to the necks enhancing the grain growth further. With the plasma heating and the DC pulsing, the particles are evenly distributed throughout the surface of the newly sintered alloy [34]. A schematic of an SPS device can be seen in Figure 12. Schematic of a typical SPS device used in surface alloy manufacturing.

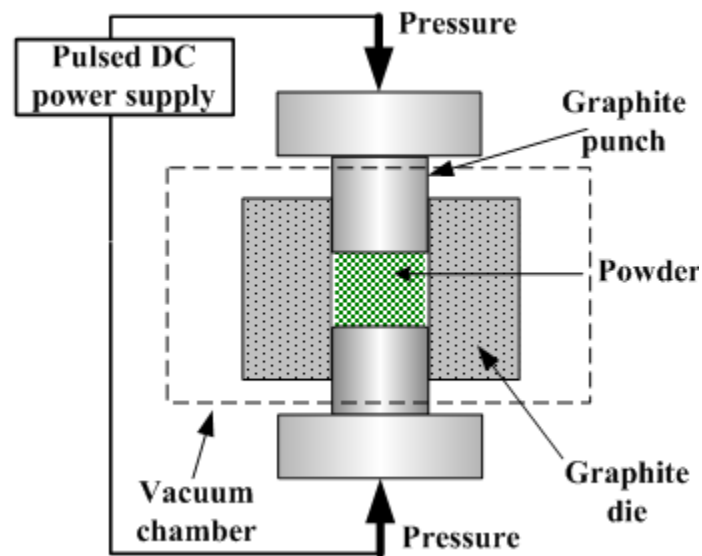


Figure 12. Schematic of a typical SPS device used in surface alloy manufacturing [34].

In reference to mechanical and thermodynamic properties, DS-W alloys have been shown to have a higher hardness at room temperature, higher tensile strength at room temperature, a lower DBTT, irradiation resistance, and crack resistance [35] [36]. These alloys are currently being investigated for their retention of deuterium and helium implantation and movement within the bulk post irradiation. It has been shown that in TiC and TaC DS-W alloys that there are surface morphology changes like fuzz and pores under low energy He irradiation at high temperatures, but the influence of the dispersoids on He bubble growth, nucleation, and capture has remained unclear

[37]. The following experiment hopes to look into the interactions that the presence of second phase carbides has on He bubble nucleation and movement within the alloy's surface.

Chapter 3

Experiment and Methods

In this chapter, the experimental procedure for the investigation of He bubble nucleation in second phase carbides will be outlined and discussed.

3.1 Material and Experimental Methods

The experimental work presented investigated the areal helium bubble density in the W matrix at different fluences of helium ion irradiation. The investigated alloy was a 5 wt. percent DS-W-TaC alloy manufactured via SPS. The alloy was FIB cut into a lamella and then polished as seen in Figure 13 and observed in an *in-situ* Transmission Electron Microscope (TEM) at the MIAMI facility at the University of Huddersfield. The DS-W alloy was ramped up in temperature to 950°C (1223K) and exposed to relatively high energy 2keV He⁺ ions at a flux of 6.77E13 ions/cm²s. The high energy He⁺ were used to induce radiation damage effects that might occur within a fusion reactor from ions colliding with the surface at higher energies than W's lattice binding energy.

Measurements of the areal He bubble density were taken both by hand and through the image manipulation software ImageJ with the counts between the two averaged at four different He⁺ radiation fluences and at four different locations of the lamella each with varying grain sizes, geometries, and densities. The four regions can be seen in Figure 14. The presence of He bubbles was also investigated in the TaC dispersoids.

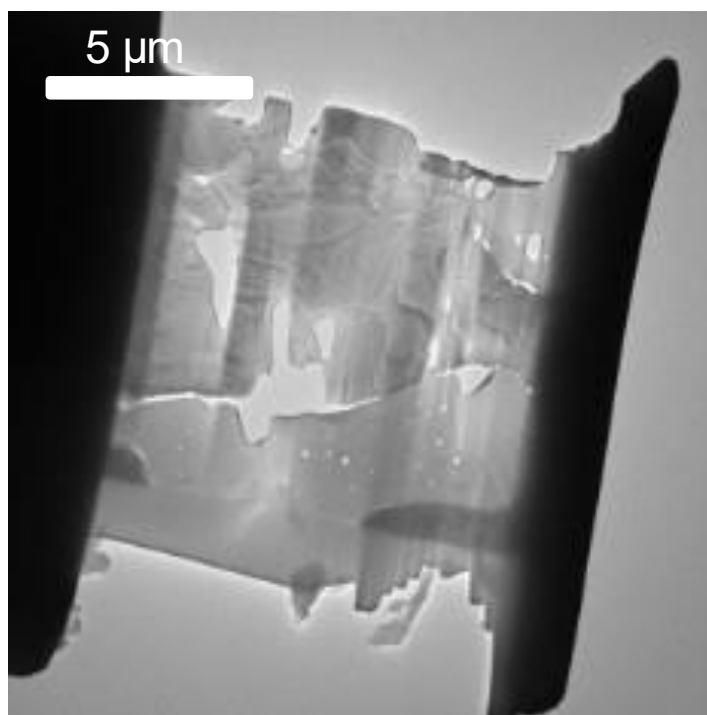


Figure 13. DS-W lamella used for the *in-situ* helium ion irradiation experiment.

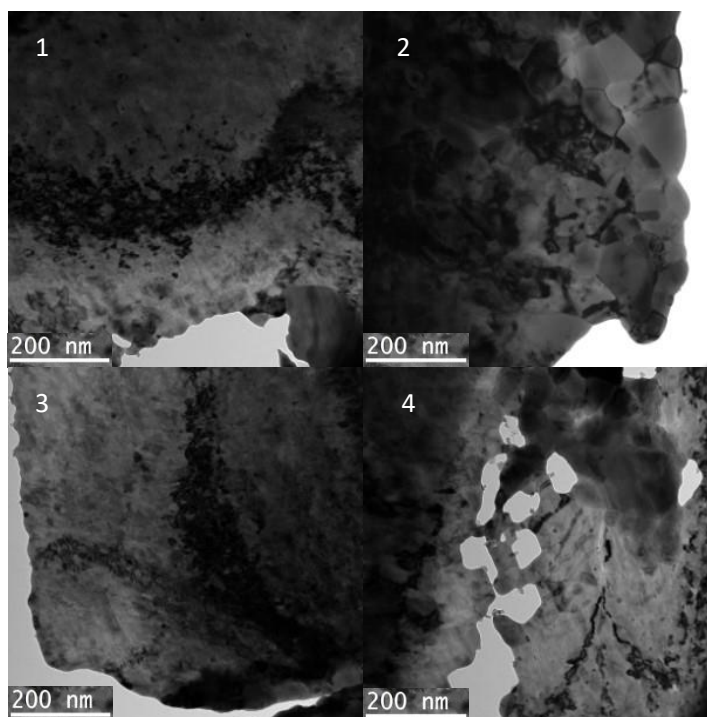


Figure 14. The four different locations investigated for areal helium bubble density. Area 1 has one visible grain boundary and W bulk, Area 2 consists of high density W-W grain boundaries, Area 3 is mostly W bulk with no visible grains, and Area 4 consists of pores in the lamella along with W-W grain boundaries.

Chapter 4

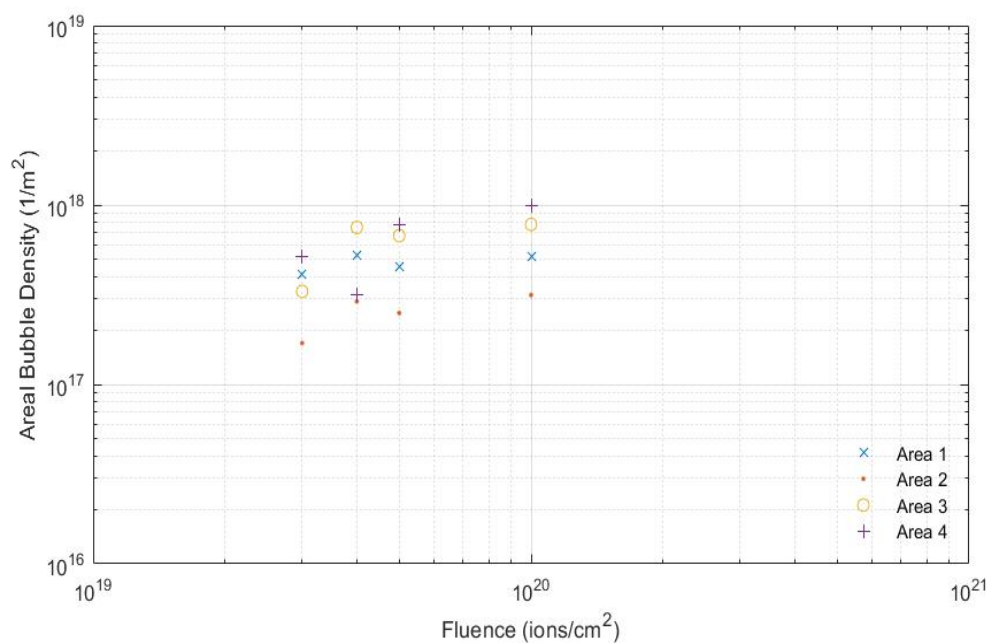
Results and Discussion

All areas exposed during the irradiation exhibited He bubble nucleation after initial irradiation. Table 1 shows the area He bubble density at each area and at each given fluence and Figure 15 visualizes this data.

He bubble nucleation was seen at all stages of fluence and at all of the Areas of interest described in the previous section. As expected, bubbles began nucleating and are only 1-2 nm in size. As fluence increases to $4E15$ ions/cm², the density of He bubbles increased for each region while the size of the largest bubbles grew to around 10 nm in diameter. At the next step of fluence, $5E15$ ions/cm², Areas 1, 2, and 3 exhibited a decrease in areal bubble density while Area 4 continued the increasing trend. These local maxima may be attributed to the increased He migration and attraction to the bubbles already established in the DS-W-TaC alloy. This would explain the large increase in bubble size observed in between irradiation steps 2 and 3 where the largest bubbles pictured reached sizes of 15-20 nm. Area 4 has some pores already established, so the smaller He bubbles could have migrated through the surface and out of the bulk instead of migrating to the larger bubbles. This likely contributed in the overall smaller bubble size seen in Area 4 as the largest bubbles are still under 5 nm in diameter – about 4 times smaller than the largest bubbles seen in the other 3 regions as seen in Figure 20. At the last fluence step, the upward trend in bubble density continued for all four of the regions with the largest bubble size remaining between 15-20 nm in diameter. The trend of bubble growth in each Area can be seen in Figure 16, Figure 17, Figure 18, Figure 19 for Areas 1, 2, 3, and 4 respectively.

Table 1. Areal Bubble Densities for Each Chosen Area

Fluence (ions/cm ²)	Areal Helium Bubble Density (1/m ²)			
	Area 1	Area 2	Area 3	Area 4
3E15	4.1	1.7	3.3	5.15
4E15	5.25	2.9	7.5	3.15
5E15	4.55	2.5	6.75	7.8
1E16	5.15	3.15	7.80	10

**Figure 15. Figure of Areal Helium Bubble Density vs. Ion Fluence.**

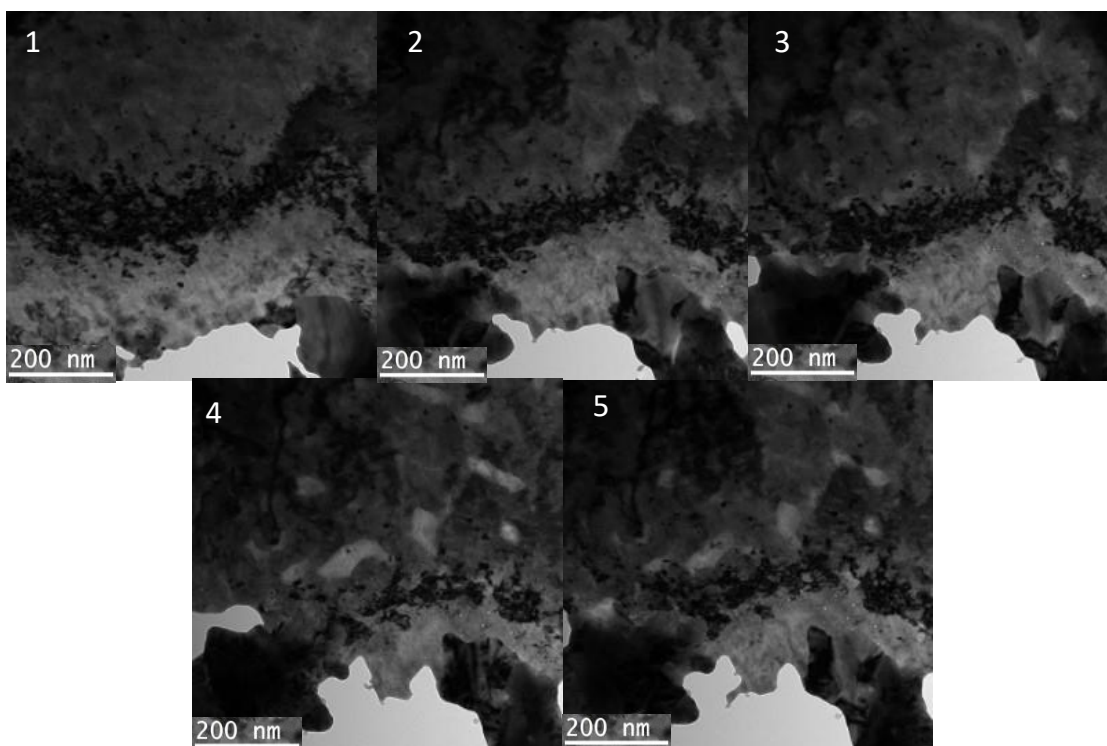


Figure 16. Area 1 Evolution for each fluence step starting at 0 ions/cm².

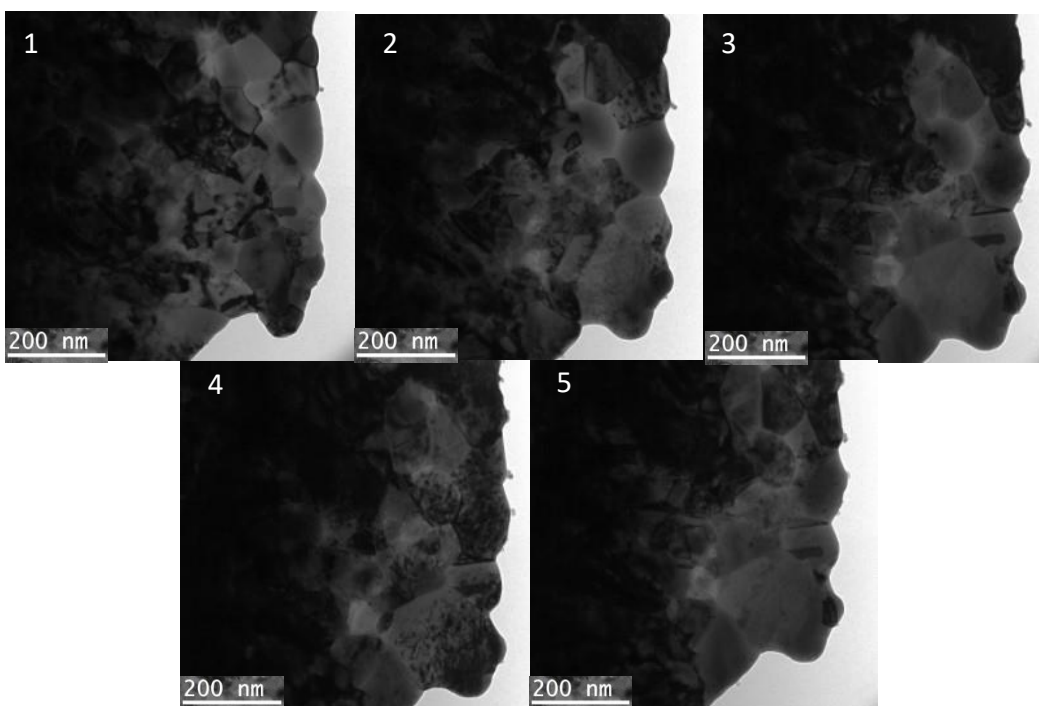


Figure 17. Area 2 Evolution for each fluence step starting at 0 ions/cm² (Images enhanced with +20% brightness and -40% contrast).

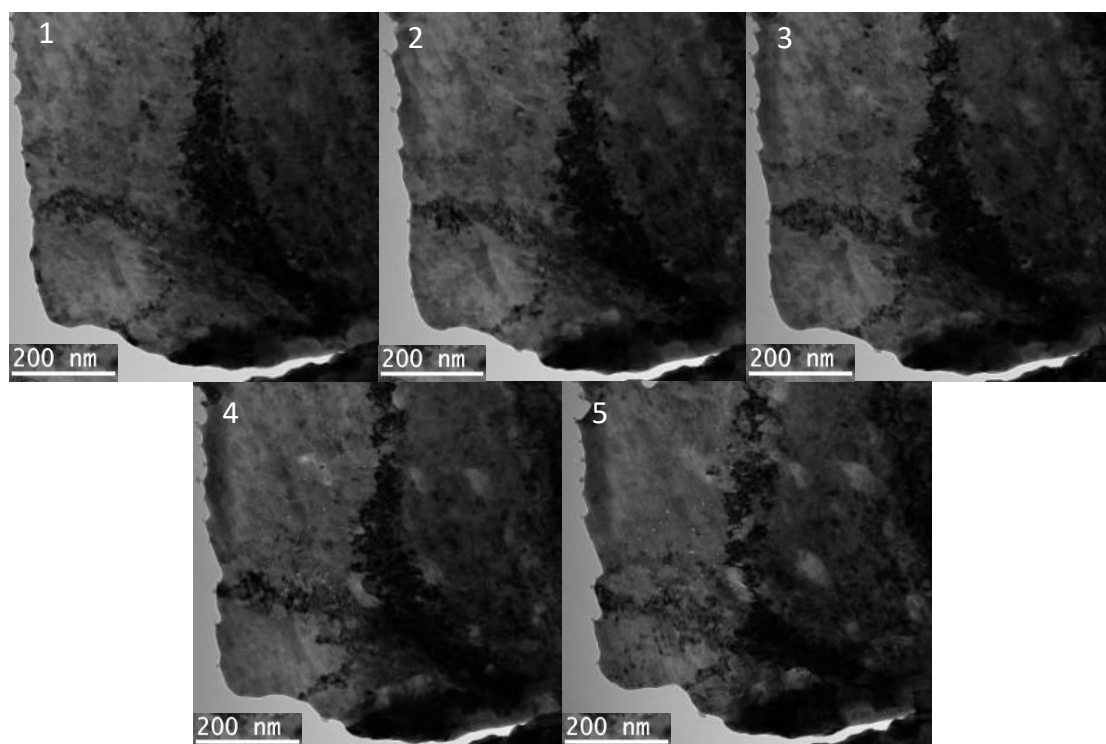


Figure 18. Area 3 Evolution for each fluence step starting at 0 ions/cm²

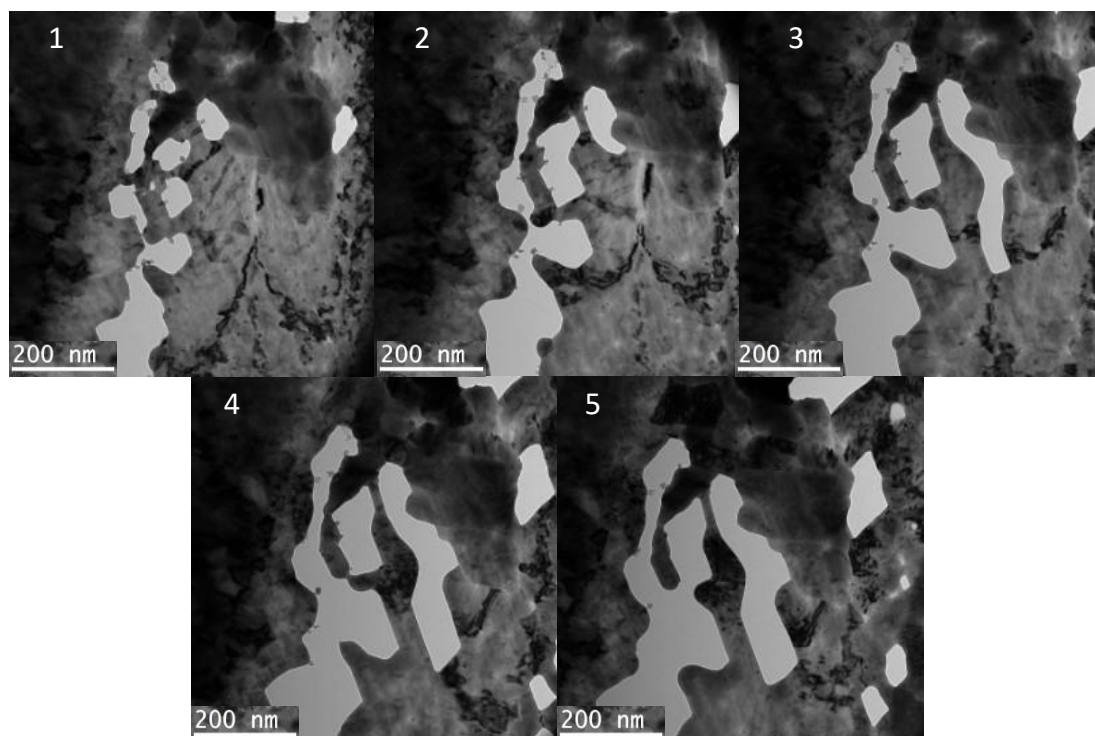


Figure 19. Area 4 Evolution for each fluence step starting at 0 ions/cm²

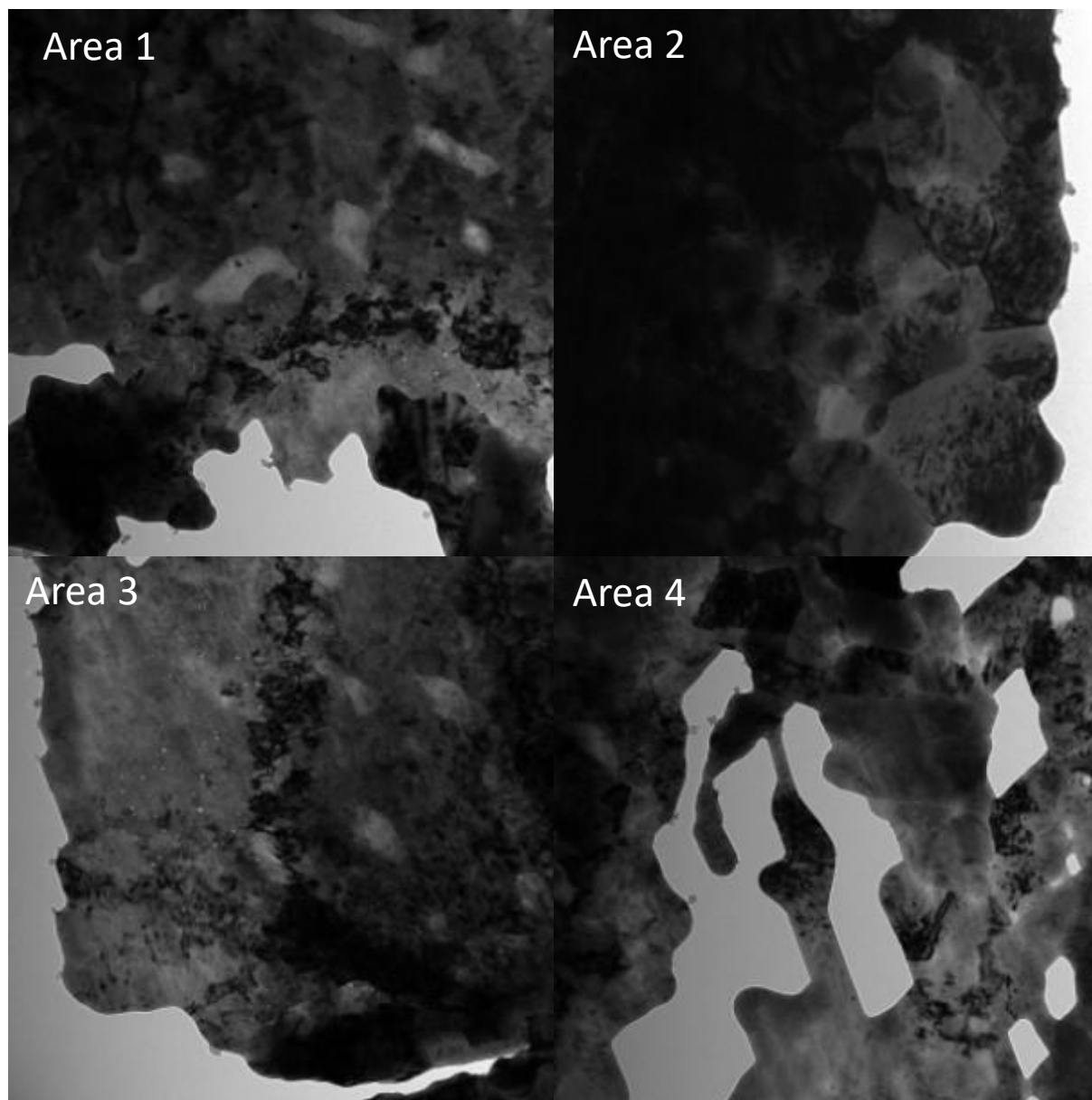


Figure 20. Each Area at the maximum fluence of 1E16 ions/cm². Area 4 has noticeably smaller bubbles than the other 3 Areas (Area 2 was changed to have +20% brightness and -40% contrast).

Using the maximum fluence step as a reference, bubble nucleation and migration was preferred along the W-W grain boundaries as seen in Figure 21. The intragranular areas near the boundaries have localized low areal densities of He bubbles while intragranular areas far from

grain boundaries have an even areal distribution of He bubbles at the maximum fluence as seen in Figure 10.

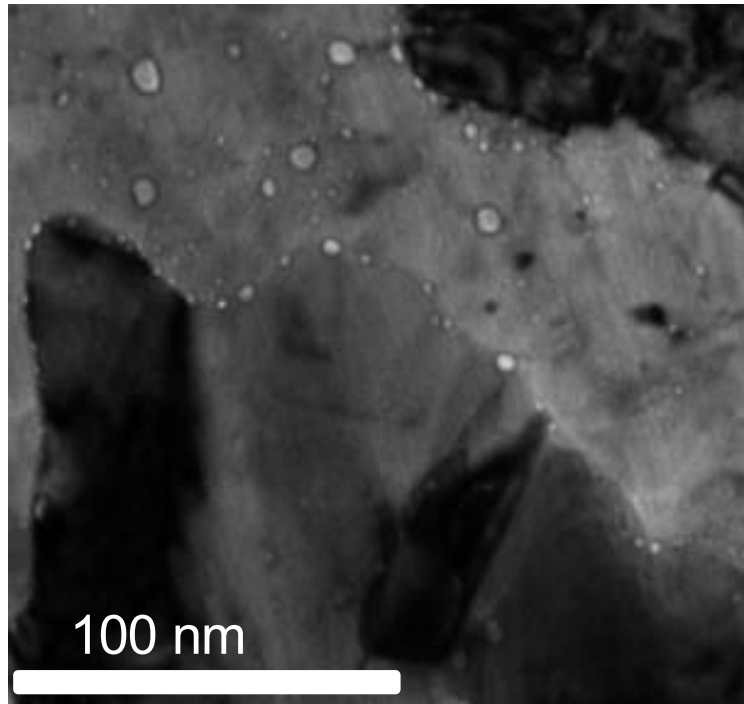


Figure 21. Helium bubble growth and migration is more common at the W-W grain boundaries as seen in this snip from Area 1.

The presence of TaC dispersoids did not seem to affect the W-W grains and the W matrix as a whole; however, within the TaC dispersoids themselves, He bubble nucleation was not present as seen in Figure 22.

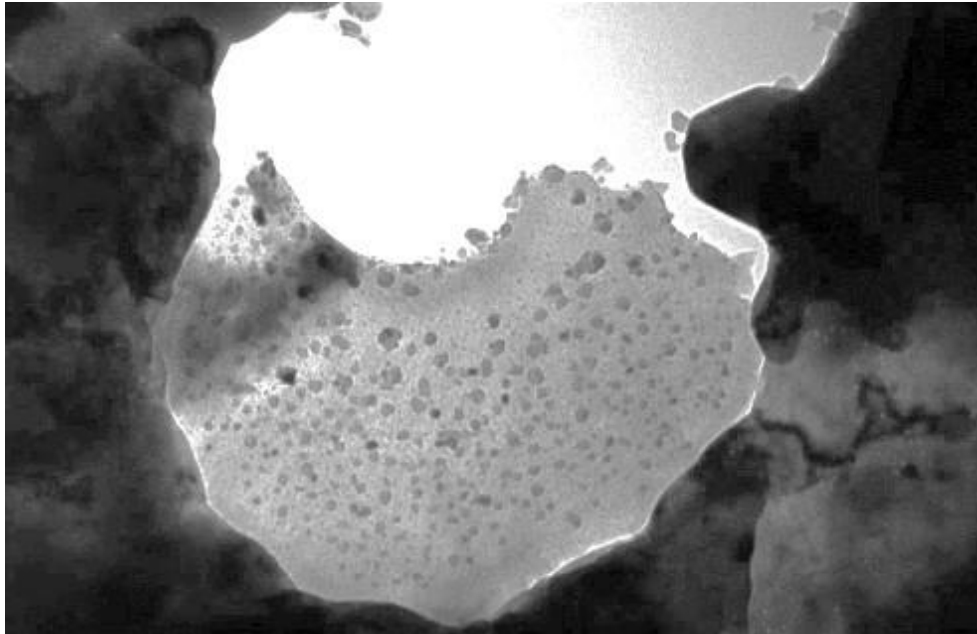


Figure 22. TaC dispersoid within the DS-W-TaC alloys used in the experiment. There are no obvious helium bubbles within it, but they can be seen in the surrounding tungsten.

Despite the presence of dispersoids in the alloy, nanofibers were created due to the expulsion of He from the bulk of the W as seen in Figure 23.

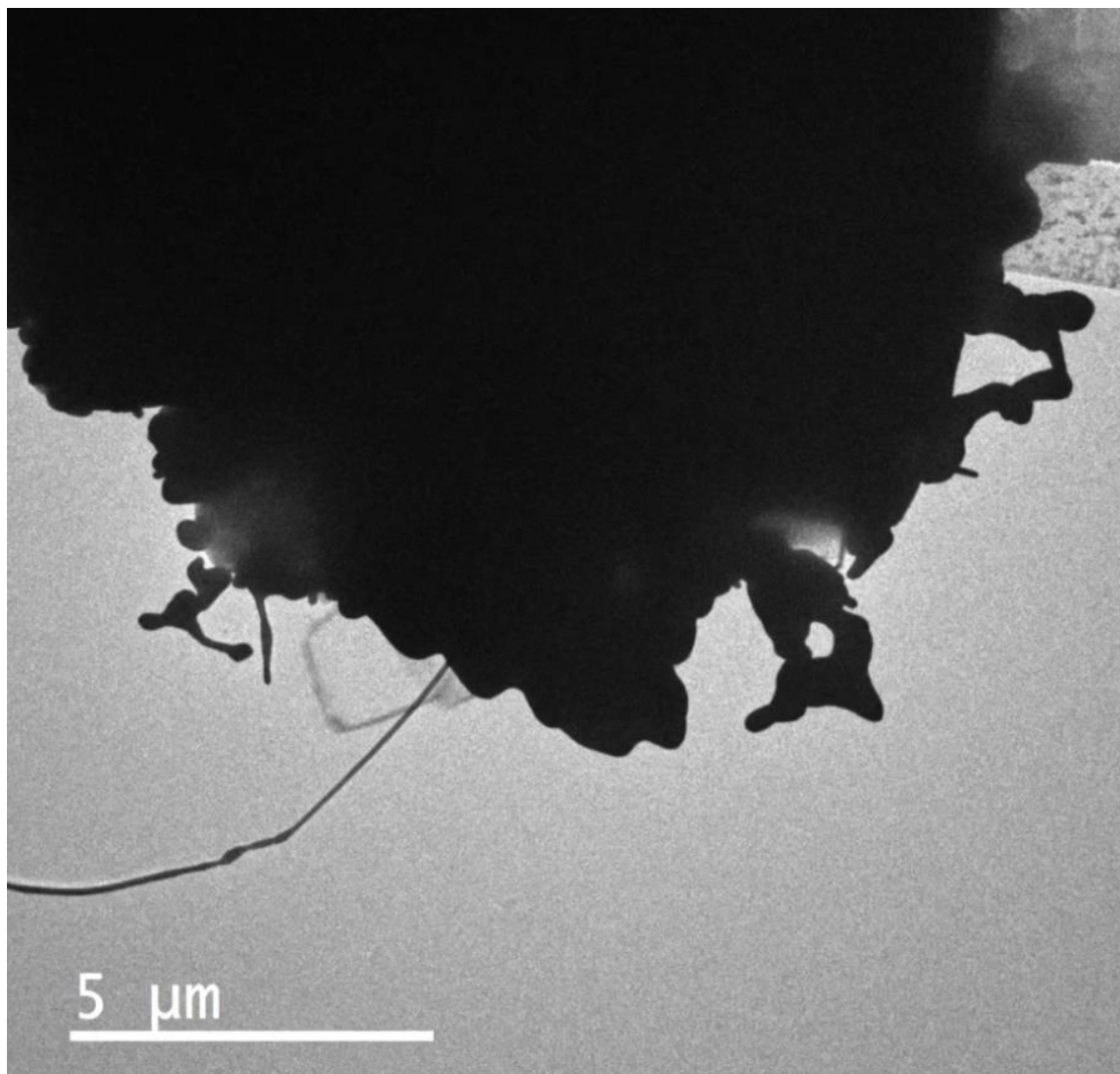


Figure 23. W nanofiber growth on the specimen.

Chapter 5

Summary and Conclusions

The behavior of helium bubble nucleation and growth within dispersion-strengthened W materials has been studied and has led to little conclusions about the effect the second phase carbides have on the overall bubble nucleation and expulsion process due past experiments developing thick impurity layers which prevent proper analysis [33].

This experiment looked into the overall influences of the second phase carbides in the tungsten bulk and focused on helium bubble nucleation and growth in intragranular W and along W-W grain boundaries with some observations regarding bubble nucleation within the TaC dispersoids themselves using an *in-situ* TEM helium ion irradiation technique at the MIAMI-I facility at the University of Huddersfield. The specimens were observed under a constant He⁺ ion flux of 6.77E13 ions/cm²s at a temperature of 950°C with He⁺ ions of 2 keV. It was found that the overall presence of the dispersoids did lower the overall bubble density of the specimen, but local He bubble densities are similar to that of pure W [38]. Despite this overall decrease, W nanofiber growth is still present in on the lamella which will interfere with the desired heat transfer properties and PMI properties that the DS-W alloys have. However, the dispersoids themselves show no sign of helium bubble nucleation.

Although this study offers an approach to the investigation of He bubble nucleation via simulating knock-on ion damage and potential helium implantation in a reactor, future studies will use He energies closer to those found within tokamaks reactors like ITER [33]. It is a point of interest that He bubble formation is absent within the TaC dispersoids themselves and warrants more investigation into how different weight percents of the carbide can affect the aggregate behavior of the alloy along with different species of second phase carbides such as ZrC and TiC.

References

- [1] J. Hanania, A. Sheardown, K. Stenhouse and J. Donev, "Nuclear Fusion in the Sun," 16 June 2020. [Online]. Available: https://energyeducation.ca/encyclopedia/Nuclear_fusion_in_the_Sun. [Accessed 15 February 2022].
- [2] S. Krikorian, "IAEA Releases Country Nuclear Power Profiles 2017," 15 March 2018. [Online]. Available: <https://www.iaea.org/newscenter/news/iaea-releases-country-nuclear-power-profiles-2017>. [Accessed 2 March 2022].
- [3] "Fission and Fusion: What is the Difference?," Office of Nuclear Energy, 1 April 2021. [Online]. Available: <https://www.energy.gov/ne/articles/fission-and-fusion-what-difference>. [Accessed 12 February 2022].
- [4] "Fusion Machines," American Physical Society, 2022. [Online]. Available: <https://www.physicscentral.com/explore/action/fusion.cfm>. [Accessed 15 March 2022].
- [5] W. M. Stacey, Fusion: An Introduction to the Physics and Technology of Magnetic Confinement Fusion, 2nd Edition, Wiley, 2010.
- [6] "Solar System Exploration," NASA, 30 March 2022. [Online]. Available: <https://solarsystem.nasa.gov/solar-system/sun/overview/>. [Accessed 15 March 2022].
- [7] M. A. Lieberman and A. J. Lichtenberg, Principles of Plasma Discharges and Materials Processing, New York: John Wiley & Sons, Inc, 1994.
- [8] "Wikicommons," 18 August 2009. [Online]. Available: https://en.wikipedia.org/wiki/File:Fusion_rxnrate.svg. [Accessed 15 March 2022].

- [9] M. Lanctot, "DOE Explains ... Nuclear Fusion Reactions," Office of Science US Department of Energy, [Online]. Available: <https://www.energy.gov/science/doe-explainsnuclear-fusion-reactions>. [Accessed 12 February 2022].
- [10] "Nuclear Fusion Power," World Nuclear Association, August 2021. [Online]. Available: <https://world-nuclear.org/information-library/current-and-future-generation/nuclear-fusion-power.aspx>. [Accessed 12 February 2022].
- [11] "Inertial Confinement Fusion: How to Make a Star," Lawrence Livermore National Laboratory, 19 October 2017. [Online]. Available: <https://lasers.llnl.gov/science/icf>. [Accessed 12 February 2022].
- [12] J. Wesson, Tokomaks 3rd Edition, Oxford: Clarendon Press, 2004.
- [13] "MAGNETS," ITER Organization, 2022. [Online]. Available: <https://www.iter.org/mach/Magnets>. [Accessed 12 February 2022].
- [14] I. Communication, "IT'S NOW OFFICIAL: FIRST PLASMA IN DECEMBER 2025," ITER, 20 June 2016. [Online]. Available: <https://www.iter.org/newsline/-/2482>. [Accessed 13 February 2022].
- [15] "REACHING 150,000,000 degrees C," ITER, [Online]. Available: <https://www.iter.org/sci/PlasmaHeating>. [Accessed 12 February 2022].
- [16] R. A. Pitts, "Physics basis for the first ITER tungsten divertor," *Nuclear Materials and Energy*, vol. 20, no. 100696, 2019.
- [17] H. Peraza Rodriguez, *Free boundary extension of the SIESTA code and its application to the Wendelstein 7-X*, Madrid: Universidad Carlos III de Madrid, 2018.

- [18] R. Maingi, S. J. Zinkle and M. S. Foster, "Report on Science Challenges and Research Opportunities in Plasma Materials Interactions," Fusion Energy Sciences US Department of Energy, 2015.
- [19] "Melting Point of Common Metals, Alloys, & Other Materials," American Elements, 2022. [Online]. Available: <https://www.americanelements.com/meltingpoint.html>. [Accessed 20 February 2022].
- [20] O. A. Waseem and J. H. Ryu, "Tungsten-Based Composites for Nuclear Fusion Applications," in *Nuclear Material Performance*, London, United Kingdom, IntechOpen, 2016.
- [21] S. M. Qaim and C. Graca, "Neutron activation cross sections at 14.7 MeV for isotopes of tungsten," *Nuclear Physics*, pp. 317-322, 1975.
- [22] N. Yoshida, H. Iwakiri, K. Tokunaga and T. Baba, "Impact of low energy helium irradiation on plasma facing metals," *Journal of Nuclear Materials*, Vols. 337-339, no. PSI-16, pp. 946-950, 2005.
- [23] H. Foll, "5.2.1 Point Defects," University of Kiel, [Online]. Available: https://www.tf.uni-kiel.de/matwis/amat/iss/kap_5/backbone/r5_2_1.html. [Accessed 15 February 2022].
- [24] F. Sefta, K. D. Hamond, N. Juslin and B. D. Wirth, "Tungsten surface evolution by helium bubble nucleation, growth and rupture," *Nuclear Fusion*, no. 53, 2013.
- [25] G. Wright and D. G. Whyte, "Tungsten nano-tendrils growth in the Alcator C-Mod divertor," *Nuclear Fusion*, vol. 52, no. 4, 2012.
- [26] P. Fiffis, D. Curreli and D. Ruzic, "Direct time-resolved observation of tungsten nanostructured growth due to helium plasma exposure," *Materials Science*, vol. 55, 2015.

- [27] M. Yajima and N. Ohno, "Tritium retention in nanostructured tungsten with large effective surface area," *Journal of Nuclear Materials*, vol. 438, pp. S1142-S1145, 2013.
- [28] D. Nshijima and R. D. J. H. Y. J. H. Baldwin, "Sputtering properties of tungsten 'fuzzy' surfaces," *Journal of Nuclear Materials*, vol. 415, pp. S96-S99, 2011.
- [29] S. Takamura, T. Miyamoto and N. Ohno, "Power transmission factor for tungsten target w/wo fiber-form nanostructure in he plasmas with hot electron component using compact plasma device ait-pid," *Fusion Science Technology*, vol. 63, p. 225, 2013.
- [30] S. Kajita, T. Yagi, K. Kobayashi, M. Tokitani and N. Ohno, "Measurement of heat diffusion across fuzzy tungsten layer," *Results in Physics*, vol. 6, pp. 877-878, 2016.
- [31] O. El-Atwani and A. Hassanein, "Helium bubble formation in ultrafine and nanocrystalline tungsten under different extreme conditions," *Journal of Nuclear Material*, vol. 458, pp. 216-223, 2015.
- [32] O. El-Atwani and E. Martinex, "Outstanding radiation resistance of tungsten-based high-entropy alloys," *Materials Science*, vol. 5, no. 3, 2019.
- [33] E. Lang, A. Kapat, T. W. Morgan and J. P. Allain, "High Flux Helium Irradiation of Dispersion-Strengthened Tungsten Alloys and Effects of Heavy Metal Impurity Layer Deposition," *Journal of Nuclear Materials*, vol. 544, 2021.
- [34] D. Kopeliovich, "Spark plasma sintering," SubsTech, 20 July 2021. [Online]. Available: https://www.substech.com/dokuwiki/doku.php?id=spark_plasma_sintering. [Accessed 30 March 2022].
- [35] X. Zhuoming and L. Changsong, "Microstructure and Mechanical Properties of Nano-Size Zirconium Carbide Dispersion Strengthened Tungsten Alloys Fabricated by Spark Plasma Sintering Method," *Plasma Science and Technology*, vol. 17, no. 12, 2015.

- [36] E. Lang, C. N. Taylor and J. P. Allain, "GD-OES Study of the influence of second phase particles on the deuterium depth distribution in dispersion strengthened tungsten," *Journal of Nuclear Materials*, vol. 532, 2020.
- [37] E. Lang, A. Kapat, T. W. Morgan and J. P. Allain, "High Flux Helium Irradiation of Dispersion-Strengthened Tungsten Alloys and Effects of Heavy Metal Impurity Layer Deposition," *Journal of Nuclear Materials*, vol. 544, 2021.
- [38] M. Miyamoto and A. Sagara, "Systematic investigation of the formation behavior of helium bubbles in tungsten," *Journal of Nuclear Materials*, vol. 463, pp. 333-336, 2015.
- [39] ""Converting Mass to Energy- Mass Defect and Nuclear Binding Energy," LibreTexts, 14 August 2020. [Online]. Available: <https://chem.libretexts.org/@go/page/47074>. [Accessed 15 February 2022].
- [40] Z. Hartwig, R. Barnard, R. Lanza, B. Sorbom, P. Stahle and D. Whyte, "An in situ accelerator-based diagnostic for plasma-material interactions science on magnetic fusion devices," *The Review of Scientific Instruments*, vol. 84, no. 123503, 2013.

ACADEMIC VITA

Evan Lambert

Huntingdon Valley, PA | elambert1@outlook.com

EDUCATION

The Pennsylvania State University, Schreyer Honors College

Bachelor of Science in Nuclear Engineering; Minor in Physics

University Park, PA

Spring 2022

PERSONAL SUMMARY

An extremely passionate engineer with experience involving design, theory, and experimental analysis of nuclear and plasma engineering concepts. Quick to learn new concepts, programs, and methods in engineering/physics processes. Currently performing research in Penn State's RSSEL group with a focus on plasma material interfaces and alloy manufacturing.

PROJECTS AND RESEARCH

RSSEL Group at The Pennsylvania State University

- Analysis of second phase carbide dispersoids in tungsten for applications of ITER divertor wall layers
- Liquid lithium as a self-healing plasma facing component in fusion plasma reactors

Sandia National Laboratory, Livermore Campus

- In-Situ low energy ion spectroscopy and direct recoil spectroscopy of hydrogen and deuterium adsorption on beryllium surfaces

The Pennsylvania State University, College of Engineering

- Research on Inverse Diffusion Type PDEs
- Exploration and the Applications of Special Relativity in Electrodynamics
- Exploration of Casimir effect applications

American Physical Society Department of Plasma Physics

November 2021

- Investigating Bubble Formation in Dispersion-Strengthened Tungsten Alloys using In-Situ Methods – author
- Response of Dispersion-Strengthened Tungsten Alloys to Helium Irradiation – co-author

EXPERIENCE

The Pennsylvania State University, Abington

Abington, PA

Summer Math Tutor

June 2019-August 2019

- Assisting students with business and engineering calculus

ASSOCIATIONS

American Nuclear Society

Member

Institute of Nuclear Materials Management

Member

AWARDS

- Eleanor D. Wilson Memorial Scholarship Award *2018-2019*
- Bert Elsbach Fellowship Scholarship for Physics *2018-2019*

RELATED COURSEWORK AND SKILLS

- Vacuum Technologies (in training)
- MatLab
- Python
- Plasma Material Interactions
- Numerical Methods
- Plasma Physics
- TEM Operation (in training)
- TEM Analysis
- OpenMC
- Nuclear Reactor Physics and Simulation
- Statistical Mechanics
- Neutron Accounting

